Synthesis, Chromatographic Separation, and Stereophysical Analysis of the Homologous $[Ni_{12-x}(PMe)_x(CO)_{24-3x}]^{2-}$ Series (x = 2, 3, 4) Containing Noncentered $Ni_{12-x}P_x$ Icosahedral Cages and the $[Ni_{10}(\mu_5\text{-}PMe)_2(\mu_4\text{-}PMe)_5(CO)_{10}]^{2-}$ Dianion Containing a Structurally Unprecedented Heptacapped Pentagonal Prismatic Metal Cage: Structural, Spectroscopic, and Electrochemical Consequences Due to Replacement of $Ni(CO)_3$ Fragments with Electronically Equivalent (Isolobal) PMe Fragments

David F. Rieck,[1a] James A. Gavney, Jr., Richard L. Norman, Randy K. Hayashi, and Lawrence F. Dahl*

Contribution from the Department of Chemistry, University of Wisconsin—Madison, Madison, Wisconsin 53706. *Received April 1, 1992*

Abstract: Reactions of $[Ni_6(CO)_{12}]^{2-}$ (**1**) with $MePCl_2$ have led to the isolation of $[Ni_{10}(PMe)_2(CO)_{18}]^{2-}$ (**2**), $[Ni_9(PMe)_3(CO)_{15}]^{2-}$ (**3**), and $[Ni_8(PMe)_4(CO)_{12}]^{2-}$ (**4**) which contain noncentered $Ni_{12-x}P_x$ icosahedral cages (x = 2, 3, 4). The three members of this unparalleled series are related by the formal substitution of isolobal PMe fragments for $Ni(CO)_3$ fragments: they, like the regular noncentered $[B_{12}H_{12}]^{2-}$ icosahedron, possess 13 skeletal electron pairs. The closely related **2**, **3**, and **4** dianions were separated by column chromatography on silica gel as were two side products—$[Ni_9(PMe)_3(CO)_{14}(\mu_2\text{-}PMe_2)]^-$ (**5**) and $[Ni_{10}(\mu_5\text{-}PMe)_2(\mu_4\text{-}PMe)_5(CO)_{10}]^{2-}$ (**6**). The electronically equivalent **5** contains a dimethylphosphido ligand in place of one doubly bridging carbonyl ligand and one negative charge in **3**. The structurally unprecedented pseudo-D_{5h} $Ni_{10}P_7$ cage in **6** contains a completely bonding electron-precise pentagonal prism of nickel atoms with its two pentagonal and five rectangular faces capped by methylphosphinidene ligands. X-ray crystallographic studies of **2**, **3**, and **4** revealed a geometric change from the squashed cylindrical 1,12-$Ni_{10}P_2$ icosahedral cage in **2** toward the more spherical 1,2,12-Ni_9P_3 cage in **3** and 1,2,9,12-Ni_8P_4 cage in **4**; this geometrical alteration is evidenced by a convergence of the (icosahedral center)-to-(cage atom) distances on going from the pseudo-D_{5d} $Ni_{10}P_2$ cage in **2** to the pseudo-C_s Ni_9P_3 cage in **3** and then to the pseudo-D_{2h} Ni_8P_4 cage in **4**. Other trends among these three icosahedral dianions are as follows: (1) IR spectra exhibiting a linear decrease in terminal carbonyl frequency, presumably due to enhanced Ni($d\pi$)–CO(π^*) backbonding; (2) cyclic voltammograms displaying irreversible or quasireversible oxidations indicating that it is hardest to oxidize **2** and easiest to oxidize **4**; and (3) $^{31}P\{^1H\}$ NMR spectra showing a general upfield shift. These trends are consistent with the homolog containing the greater number of PMe fragments being more electron-rich such that the electron-density surface charge on the $Ni_{12-x}P_x$ icosahedral cage (x = 2, 3, 4) is largest for **4** (x = 4) and smallest for **2** (x = 2). The $^{31}P\{^1H\}$ NMR solution spectra of $Ni_{10}P_2$ **2** and Ni_8P_4 **4** give no insight concerning possible nonrigidity of their cage frameworks in solution. Fluxional behavior of the $Ni_{12-x}P_x$ cages on the NMR time scale is excluded on the basis of virtually identical $^{31}P\{^1H\}$ NMR spectra of Ni_9P_3 **3** at 22 and 50 °C exhibiting three well-resolved phosphorus signals with an ABX pattern that conforms to the solid-state structure. The following salient structural features emerge from the single-crystal X-ray diffraction studies: (1) **2** possesses crystallographic C_i-$\bar{1}$ site symmetry and an experimentally equivalent configuration in each of its three salts; the same carbonyl arrangement of 10 terminal, four doubly bridging, and two triply bridging carbonyl ligands markedly affects the Ni–Ni bond lengths such that the pseudosymmetry of the centrosymmetric $Ni_{10}P_2$ cage is reduced from D_{5d} to C_{2h}-2/m. (2) **3** has crystallographic C_1-1 site symmetry and an overall pseudo-C_s symmetry in each of its two salts. Although the overall disposition of nine terminal and six bridging carbonyl ligands is the same, there are marked differences in the Ni–CO(bridging) distances for the bridging carbonyl ligands. This alteration in bridging carbonyl linkage to the Ni_9P_3 icosahedra of **3** in the two salts is attributed to dissimilar crystallographic packing interactions. (3) **4** in the $[PPh_3Me]^+$ salt has crystallographic C_i-$\bar{1}$ site symmetry and approximately conforms to D_{2h}-mmm symmetry with eight terminal and four asymmetrically-coordinated triply-bridging carbonyl ligands.

Introduction

The regular noncentered icosahedron, a 12-vertex Platonic solid[2] of I_h symmetry (i.e., with 12 C_5, 10 C_3, and 15 C_2 axes and a center of symmetry i) which possesses 20 triangular faces and 30 edges, was first established as an important discrete architectural unit from theoretical[3] and experimental[4] studies of the classic $[B_{12}H_{12}]^{2-}$ dianion. This deltahedron, which may be envisioned as a bicapped pentagonal antiprism, has emerged as a fundamental building block in solid-state materials such as several allotropes of elemental boron,[5] complex borides,[5,6] gallides,[6,7] and quasicrystalline aluminum alloys.[8] The existence of an icosahedral geometry in

(1) Present address: Salisbury State University, Salisbury, MD 21801.
(2) Wells, A. F. *Structural Inorganic Chemistry*, 5th ed.: Oxford University Press: London, 1984; pp 69–71.
(3) (a) Longuet-Higgens, H. C.; Roberts, M. de V. *Proc. R. Soc. (London), Ser. A* **1955**, *230*, 110–119. (b) Hoffmann, R.; Lipscomb, W. N. *J. Chem. Phys.* **1962**, *36*, 2179–2189.
(4) (a) Lipscomb, W. N.; Wunderlich, J. A. *J. Am. Chem. Soc.* **1960**, *82*, 4427–4428. (b) Pilochelli, A. R.; Hawthorne, M. F. *J. Am. Chem. Soc.* **1960**, *82*, 3228–3229. (c) Muetterties, E. L.; Merrifield, R. E.; Miller, H. C.; Knoth, Jr., W. H.; Downing, J. R. *J. Am. Chem. Soc.* **1962**, *84*, 2506–2508.
(5) (a) Hoard, J. L.; Hughes, R. E. *The Chemistry of Boron and its Compounds*; Muetterties, E. L., Ed.; J. Wiley & Sons, Inc.: New York, 1967; Chapter 2, pp 25–154.
(6) Burdett, J. K.; Canadell, E. *J. Am. Chem. Soc.* **1990**, *112*, 7207–7217.
(7) (a) Schäfer, H. *J. Solid-State Chem.* **1985**, *57*, 97–111. (b) Belin, C.; Ling, R. G. *J. Solid-State Chem.* **1983**, *48*, 40–48. (c) Belin, C.; Charbonnel, M. *J. Solid-State Chem.* **1986**, *64*, 57–66. (d) Charbonnel, M.; Belin, C. *J. Solid-State Chem.* **1987**, *67*, 210–218. (e) King, R. B. *Inorg. Chem.* **1989**, *28*, 2796–2799.
(8) King, R. B. *Inorg. Chim. Acta* **1991**, *181*, 217–225 and references therein.

0002-7863/92/1514-10369$03.00/0

extended solids is remarkable. While ccp and hcp configurations of metal atoms in a number of high-nuclearity metal clusters may be described as fragments of bulk metals,[9] icosahedral growth by metal layering is crystallographically incompatible (due to 5-fold symmetry) with translational periodicity in ordered crystalline materials. Nevertheless, centered icosahedra have been implicated as structural units in a wide variety of amorphous materials[10] (including certain Ni–P alloys) and in the formation and growth of small metal particles.[11] Several theoretical investigations have been performed on centered metal icosahedra,[12] and it has been shown for normally face-centered cubic materials such as nickel metal that the mininum energy-packing configuration is the centered 13-atom icosahedron.[10a] The metal configurations of an extensive series of Au–Ag "supraclusters" have been described by Teo and Zhang[13] in terms of modular systems based upon the vertex sharing of 13-atom Au-centered icosahedra.

The first crystallographically characterized examples of discrete nonboron-containing transition-metal clusters with centered icosahedral metal cores are the $[Au_{13}(PPhMe_2)_{10}Cl_2]^{3+}$ trication,[14-16] which has a Au-centered Au_{12} icosahedral cage, and the $[Rh_{12}Sb(CO)_{27}]^{3-}$ trianion,[17,18] which has an Sb-centered Rh_{12} icosahedral cage. The methylarsinidene $[Ni_{10}(AsMe)_2(CO)_{18}]^{2-}$ and phenylarsinidene $[Ni_9(AsPh)_3(CO)_{15}]^{2-}$ dianions,[19] prepared and structurally characterized in our laboratories, represent the first examples of discrete, nonboron-containing clusters with noncentered $Ni_{10}As_2$ and Ni_9As_3 icosahedral cages. These studies led us to examine the reactions of $MePCl_2$ with the $[Ni_6(CO)_{12}]^{2-}$ dianion (**1**)[20] as the $[NMe_4]^+$ salt in THF at room temperature;[21] two products were isolated—viz., the $[Ni_{10}(PMe)_2(CO)_{18}]^{2-}$ dianion (**2**), which was characterized both as the acetone-solvated $[Ph_3PNPPh_3]^+$ salt (**2b**) and the $[NMe_4]^+$ salt (**2c**), and the $[Ni_9(PMe)_3(CO)_{15}]^{2-}$ dianion (**3**), which was characterized as the cyclohexane-solvated $[NMe_4]^+$ salt (**3b**). In this earlier work,[21] only solvent extractions and metathesis counterion reactions were used to separate the anionic products. Consequently, samples of **3** were invariably contaminated with **2**; pure **3** as the $[NMe_4]^+$ salt was obtained in the Pasteur fashion by crystal separation under a microscope. The $[Ni_{10}(SbPh)_2(CO)_{18}]^{2-}$ dianion was subsequently prepared from reactions of **1** with Ph_2SbCl or $PhSbCl_2$.[22]

Complementary work by Longoni and co-workers[23,24] has produced several important related clusters including the $[Ni_{12}E(CO)_{22}]^{2-}$ dianions (E = Sn, Ge)[24] with E-centered Ni_{12} icosahedral cages and the recently isolated $[Ni_{11}(ENi(CO)_3)_2(CO)_{18}]^{n-}$ anions (E = Sb,[25] Bi;[26] n = 2, 3, 4) with Ni-centered $Ni_{10}E_2$ cages.

Until recently, the use of chromatographic separation techniques for the isolation of pure samples of high-nuclearity metal cluster anions was essentially unknown.[27,28] Primarily as a consequence of our development of column chromatographic procedures under anaerobic conditions for the separation of complicated product mixtures of platinum carbonyl clusters,[29] it became apparent that column chromatography on silica gel support could be used to isolate and identify the products arising from the reaction of **1** with $MePCl_2$. Herein are given the details of the synthesis, chromatographic separation, and characterization not only of **2** and **3** but also of three initially undetected clusters—viz., the $[Ni_8(PMe)_4(CO)_{12}]^{2-}$ dianion (**4**), which is the third member of the homologous $[Ni_{12-x}(PMe)_x(CO)_{24-3x}]^{2-}$ series (x = 2, 3, 4), and the $[Ni_9(PMe)_3(CO)_{14}(\mu_2\text{-}PMe_2)]^-$ monoanion (**5**) and $[Ni_{10}(PMe)_7(CO)_{10}]^{2-}$ dianion (**6**), which are side-products of structural interest. In fact, **6** is the first example of a heptacapped pentagonal prismatic metal cluster of pseudo-D_{5h} symmetry. The isolation of these five similar anionic products by the use of silica gel and chromatographic equipment adapted to Schlenk techniques provides an illustration of the advantages of conventional silica gel supports over extraction-metathesis procedures for separating this complex mixture of anionic metal clusters.

The work for this series of three $Ni_{12-x}(PMe)_x$ icosahedral clusters (x = 2, 3, 4) evolved into accomplishing two major objectives: (1) X-ray crystallographic, spectroscopic, and electrochemical studies in order to examine the stereophysical effects caused by a sequential replacement of two $Ni(CO)_3$ fragments by two sterically less-demanding isolobal[30] PMe fragments; and (2) an assessment of the $^{31}P\{^1H\}$ NMR spectra to determine whether these clusters exhibit stereochemical nonrigidity of their icosahedral cage frameworks in solution. Such fluxional behavior was deemed possible, especially in light of variable-temperature NMR solution spectra indicating that the highly-distorted Sb-centered Rh_{12} icosahedral skeleton in the $[Rh_{12}Sb(CO)_{27}]^{3-}$ trianion is fluxional in acetone-d_6 at room temperature[17b] and that the para isomer of the Au-centered $[Au_{13}(PPhMe_2)_{10}Cl_2]^{3+}$ trication isomerizes in CD_2Cl_2 solution at room temperature into the alternative ortho and/or meta isomers.[14a] The results presented here have fulfilled our objectives.

The fact that neither the corresponding icosahedral *tert*-butylphosphinidene nickel clusters[31] nor the hypothetical icosahedral $[Ni_{12}(CO)_{24}]^{2-}$ dianion (which would be electronically equivalent with **2**, **3**, and **4**) is observed (vide infra) provides evidence that steric effects as well as electronic requirements play an important role in determining whether a metal cluster with an icosahedral cage can be formed. Reactions of the electronically equivalent $Ni_{12-x}E_x$ icosahedral clusters (E = P, As, Sb) with additional

(9) Kharas, K. C. C.; Dahl, L. F. Ligand-Stabilized Metal Clusters: Structure, Bonding, Fluxionality, and the Metallic State. *Adv. Chem. Phys.* **1988**, *70* (Part 2), 1–43.

(10) (a) Briant, C. L.; Burton, J. J. *Phys. Status Solidi B* **1978**, *85*, 393–402. (b) Machizaud, F.; Kuhnast, F. A.; Flechon, J. *Ann. Chim. (Paris)* **1978**, *3*, 177–186.

(11) Renou, A.; Gillet, M. *Surf. Sci.* **1981**, *106*, 27–34 and references cited therein.

(12) (a) Fripiat, G.; Chow, K. T.; Boudart, M.; Diamond, B.; Johnson, K. H. *J. Mol. Catal.* **1975**, *1*, 59–72. (b) Charlot, M. F.; Kahn, O. *Surf. Sci.* **1979**, *81*, 90–108.

(13) Teo, B. K.; Zhang, H. *Proc. Natl. Acad. Sci. U.S.A.* **1991**, *88*, 5067–5071 and references therein.

(14) (a) Briant, C. E.; Theobald, B. R. C.; White, J. W.; Bell, L. K.; Mingos, D. M. P.; Welch, A. J. *J. Chem. Soc., Chem. Commun.* **1981**, 201–202. (b) Mingos, D. M. P. *Philos. Trans. R. Soc. London, A* **1982**, *No. 308*, 75–83.

(15) The nonconformity of this icosahedral cluster to a 170-electron count corresponding to 13 skeletal electron pairs has been rationalized from different bonding models.[16]

(16) (a) Mingos, D. M. P. *J. Chem. Soc., Dalton Trans.* **1976**, 1163–1169. (b) Briant, C. E.; Hall, K. P.; Wheeler, A. C.; Mingos, D. M. P. *J. Chem. Soc., Chem. Commun.* **1984**, 248–250. (c) King, R. B. *Inorg. Chim. Acta* **1986**, *116*, 109–117.

(17) (a) Vidal, J. L.; Troup, J. M. *J. Organomet. Chem.* **1981**, *213*, 351–363. (b) Heaton, B. T.; Strona, L.; Pergola, R. D.; Vidal, J. L.; Schoening, R. C. *J. Chem. Soc., Dalton Trans.* **1983**, 1941–1947.

(18) Its 170 electron count corresponds to the expected 13 skeletal electron-pair count.

(19) Rieck, D. F.; Montag, R. A.; McKechnie, T. S.; Dahl, L. F. *J. Am. Chem. Soc.* **1986**, *108*, 1330–1331.

(20) (a) Calabrese, J. C.; Dahl, L. F.; Cavalieri, A.; Chini, P.; Longoni, G.; Martinengo, S. *J. Am. Chem. Soc.* **1974**, *96*, 2616–2618. (b) Longoni, G.; Chini, P.; Cavalieri, A. *Inorg. Chem.* **1976**, *15*, 3025–3029.

(21) Rieck, D. F.; Rae, A. D.; Dahl, L. F. *Abstracts of Papers*; 190th National Meeting of the American Chemical Society, Chicago, IL, Sept 1985; American Chemical Society: Washington, DC, 1985; INORG 157.

(22) DesEnfants, II, R. E.; Gavney, Jr., J. A.; Hayashi, R. K.; Dahl, L. F. *J. Organomet. Chem.* **1990**, *383*, 543–572.

(23) Longoni, G. *Pure Appl. Chem.* **1990**, *62*, 1183–1186.

(24) Ceriotti, A.; Demartin, F.; Heaton, B. T.; Ingallina, P.; Longoni, G.; Manassero, N.; Marchionna, M.; Masciocchi, N. *J. Chem. Soc., Chem. Commun.* **1989**, 786–787.

(25) (a) Albano, V. G.; Demartin, F.; Iapalucci, M. C.; Longoni, G.; Sironi, A.; Zanotti, V. *J. Chem. Soc., Chem. Commun.* **1990**, 547–548. (b) Albano, V. G.; Demartin, F.; Iapalucci, M. C.; Laschi, F.; Longoni, G.; Sironi, A.; Zanello, P. *J. Chem. Soc., Dalton Trans.* **1991**, 739–748.

(26) Albano, V. G.; Demartin, F.; Iapalucci, M. C.; Longoni, G.; Monari, M.; Zanello, P. *J. Chem. Soc., Dalton Trans.* **1992**, 497–502.

(27) The separation and identification of large cationic clusters by reverse-phase HPLC was recently reported by Pignolet and co-workers.[28]

(28) Bos, W.; Steggerds, J. J.; Yan, S.; Casalnuovo, J. A.; Mueting, A. M.; Pignolet, L. H. *Inorg. Chem.* **1988**, *27*, 948–951.

(29) Lewis, G. F.; Hayashi, R. K.; Dahl, L. F. *Abstracts of Papers* (Part 1), 3rd Chemical Congress of North America, Toronto, Canada, June 1988; American Chemical Society: Washington, DC, 1988; INORG 660.

(30) (a) Elian, M.; Chen, M. M. L.; Mingos, D. M. P.; Hoffmann, R. *Inorg. Chem.* **1976**, *15*, 1148–1155. (b) Hoffmann, R. *Science (Washington, D.C.)* **1981**, *211*, 995–1002. (c) Hoffmann, R. *Angew. Chem., Int. Ed. Engl.* **1982**, *21*, 711–724. (d) Albright, T. A. *Tetrahedron* **1982**, *38*, 1339–1388. (e) Stone, F. G. A. *Angew. Chem., Int. Ed. Engl.* **1984**, *23*, 89–99.

(31) Montag, R. A. Ph.D. Thesis, 1982, University of Wisconsin—Madison.

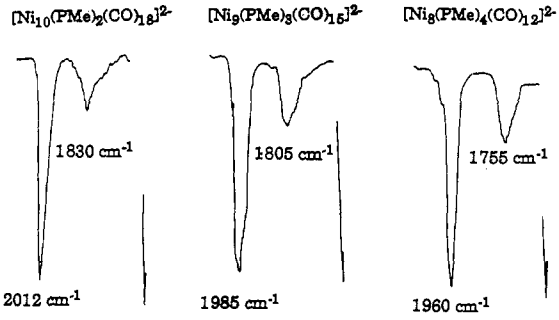

Figure 1. IR-monitored separation of $[Ni_{10}(PMe)_2(CO)_{18}]^{2-}$ (**2**), $[Ni_9(PMe)_3(CO)_{15}]^{2-}$ (**3**), and $[Ni_8(PMe)_4(CO)_{12}]^{2-}$ (**4**) via column chromatography on silica gel under N_2 atmosphere. Each IR solution spectrum was taken on the $[PPh_3Me]^+$ salt dissolved in THF under N_2.

organo (main-group) halides have given rise to other products including $Ni_8(\mu_4\text{-}PMe)_6(CO)_8$, with a hexacapped cubane-like[32] Ni_8 core, $Ni_8(PCMe_3)_2(PMe)_2(CO)_{12}$, with a tetracapped cuneane-like[33] Ni_6P_2 core, and $Ni_8(\mu_5\text{-}SbR)_2(\mu_4\text{-}PR')_2(\mu_3\text{-}PR')_2(CO)_8$ (where R = Ph, R' = CMe_3), with a hexacapped cuneane-like[33] Ni_8 core; this work will be reported elsewhere.[34]

Experimental Section

Materials and Techniques. All reactions and manipulations were carried out under an atmosphere of dry nitrogen via standard Schlenk techniques or within a Vacuum Atmospheres drybox. All solvents were dried and distilled immediately before use. All NMR spectra were obtained in acetone-d_6 which was dried, frozen, and then degassed three times and vacuum-distilled before use. The $[PPh_3Me]^+$ salt of **1** ($[PPh_3Me]^+_2[Ni_6(CO)_{12}]^{2-}$) was prepared by minor modifications of the procedure described by Longoni, Chini, and Cavalieri.[20b] Silica gel (Kieselgel 60, 230–400 mesh; Merck) was initially heated under vacuum to 150 °C for 24 h; it then was cooled to ambient temperature, after which distilled water (5% by weight) was added under N_2 to ensure consistent activity. The $PMeCl_2$ was purchased from Strem and other major chemical suppliers and used without further purification.

All ^1H NMR spectra were recorded on a Bruker WP-200 spectrometer; chemical shifts are reported relative to Me_4Si calculated from the chemical shifts of residual solvent protons. All ^{31}P NMR spectra were recorded on a Bruker AM-500 spectrometer with phosphoric acid as an external reference. Infrared spectra were recorded on a Beckman 4240 spectrophotometer.

Electrochemical measurements were performed with a Bioanalytical Systems Electrochemical Analyzer equipped with a PAR electrochemical cell which was operated inside a Vacuum Atmospheres drybox. The cell consisted of a working electrode (either glassy carbon or platinum disk), a platinum wire counterelectrode, and a saturated calomel electrode. All voltages were measured relative to the standard calomel electrode (SCE). The supporting electrolyte ($[n\text{-}Bu_4N]^+[PF_6]^-$) concentration was maintained at 0.1 M, and *iR* compensation for solution resistance[35] was made before measurement of the current versus voltage curves.

Reactions of $[Ni_6(CO)_{12}]^{2-}$ (1) with $MePCl_2$. In a typical reaction, 0.32 mL (2.08 mmol) of neat $MePCl_2$ was added dropwise via syringe to a stirring solution of **1** as the $[PPh_3Me]^+$ salt (3.00 g, 2.41 mmol) in 50 mL of THF. After 90 min the solvent was removed under vacuum. The reaction residue was extracted with toluene to yield a red-brown solution from which 0.50 g of material was isolated. Extraction of the remaining residue with THF gave a dark solution, from which 1.50 g of dark brown material was isolated by the evaporation of the solvent. After extraction with THF, the reaction residue consisted of a pale green powder, presumably $NiCl_2$. The THF extract was separated via column chromatography with 5% deactivated silica gel support. The chromatographic apparatus consisted of a 4 cm diameter by 50 cm long column with a 500 mL solvent reservoir at the top and a fritted glass disc in a Teflon flow regulator at the bottom. Optimum separation was achieved by use of an elution mixture composed of 2:1 THF/diisopropyl ether. Separation of the THF extract was monitored by IR spectroscopy (Figure 1); the Ni_9P_3 **5** was the first to elute followed by the $Ni_{10}P_7$ **6**, Ni_8P_4 **4**, Ni_9P_3 **3**, and $Ni_{10}P_2$ **2**. The **2**, **3**, and **4** dianions as the $[PPh_3Me]^+$ salts were obtained in quantities of 700, 400, and 400 mg, respectively, corresponding to yields (based on nickel) of 28, 15, and 14%, respectively. The green side-product **6** was isolated in such small quantities (estimated yield <3%) that the extracts of several syntheses were combined to obtain a sufficient amount for crystallization. The dark red side-product **5** was isolated from one reaction and structurally characterized as the $[Na(THF)_4]^+$ salt; this counterion is readily attributed to one sample of the $[PPh_3Me]^+$ salt of the reactant **1**, which was prepared by the metathesis reaction of the sodium salt of **1** with $[PPh_3Me]^+Br^-$, containing the sodium salt as an impurity. Generation of the dimethylphosphido ligand in **5** is ascribed to decomposition of the $[PPh_3Me]^+$ cation; another possible source of this ligand is the presence of Me_2PCl as an impurity in $MePCl_2$.

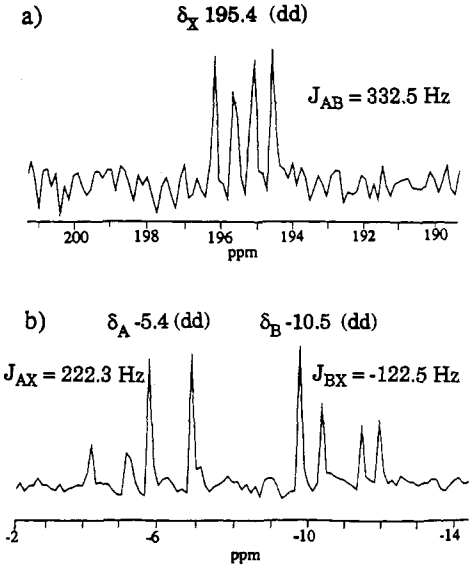

Figure 2. 202-MHz $^{31}P\{^1H\}$ NMR spectrum of $[Ni_9(PMe)_3(CO)_{15}]^{2-}$ (**3**) as the $[PPh_3Me]^+$ salt in acetone-d_6 at room temperature. Three well-resolved ^{31}P resonances are observed: (a) expanded X region; (b) expanded AB region.

The $[NMe_4]^+$ salt of **3** was isolated from an analogous reaction starting with the $[NMe_4]^+$ salt of **1**.

Characterization of $[Ni_{10}(PMe)_2(CO)_{18}]^{2-}$ (2). This air-sensitive dark brown compound was characterized as the $[PPh_3Me]^+$ salt which is soluble in THF, acetone, and acetonitrile. An infrared spectrum of **2a** in THF exhibited a strong terminal band at 2012 cm^{-1} and bridging carbonyl bands at 1830 (m) and 1770 cm^{-1} (w, sh). A cyclic voltammogram of **2a** in THF showed no reductions out to −1.5 V and an irreversible oxidation at approximately +0.75 V.

A ^1H NMR spectrum of **2a** in acetone-d_6 at 22 °C displayed an indicated triplet resonance at δ 2.40 which was assigned to the methyl protons. This triplet signal, which showed field-strength dependence, was attributed to virtual coupling. All other proton signals were due to the solvent and counterion. A $^{31}P\{^1H\}$ NMR spectrum of **2a** exhibited a single sharp peak at δ 271.9; the ^{31}P resonance at δ 22.6 was assigned to the $[PPh_3Me]^+$ monocation.

Characterization of $[Ni_9(PMe)_3(CO)_{15}]^{2-}$ (3). This air-sensitive dark orange compound was characterized as the $[PPh_3Me]^+$ salt (**3a**) and the $[NMe_4]^+$ salt (**3b**), both of which are soluble in THF and acetone. An infrared spectrum of **3a** in THF displayed a strong terminal band at 1985 cm^{-1} and a broad bridging band centered at 1805 (mw) cm^{-1}. A cyclic voltammogram of **3a** in THF showed no reductions out to −1.5 V and two inseparable quasireversible oxidation waves at approximately 0.30 V.

A ^1H NMR spectrum of **3a** at 22 °C showed signals at δ 2.21 (dd, J = 12.5, 2.5 Hz), δ 1.81 (dd, J = 12.5, 7.5 Hz) and δ 1.76 (m) which were assigned to the methyl protons. All other proton signals were due to the solvent and counterion. A $^{31}P\{^1H\}$ NMR spectrum at 22 °C displayed an ABX splitting pattern (Figure 2) with δ_A −5.4, δ_B −10.5, and δ_X 195.4 (J_{AB} = 332.5, J_{AX} = 222.3, J_{BX} = −122.5 Hz). A virtually identical spectrum was obtained at 50 °C. The ^{31}P resonance at δ 22.6 was assigned to the $[PPh_3Me]^+$ monocation.

Characterization of $[Ni_8(PMe)_4(CO)_{12}]^{2-}$ (4). This air-sensitive red compound was characterized as the $[PPh_3Me]^+$ salt (**4a**) which is soluble

(32) (a) Eaton, P. E.; Cole, T. W., Jr. *J. Am. Chem. Soc.* **1964**, *86*, 3157–3158. (b) Fleischer, E. B. *J. Am. Chem. Soc.* **1964**, *86*, 3889–3890. The name "cubane" was utilized to describe the configuration of O_h C_8H_8.

(33) Cassar, L.; Eaton, P. E.; Halpern, J. *J. Am. Chem. Soc.* **1970**, *92*, 6366–6368. The name "cuneane", adopted specifically to describe pentacyclo[3.3.0.$0^{2,4}$.$0^{3,7}$.$0^{6,8}$] which is a C_{2v} valence isomer of "cubante", is derived from the Latin "cuneus", a wedge.

(34) Gavney, Jr., J. A.; Rieck, D. F.; Montag, R. A.; Dahl, L. F. Manuscript in preparation.

(35) He, P.; Avery, J. P.; Faulkner, L. R. *Anal. Chem.* **1982**, *54*, 1313A–1326A.

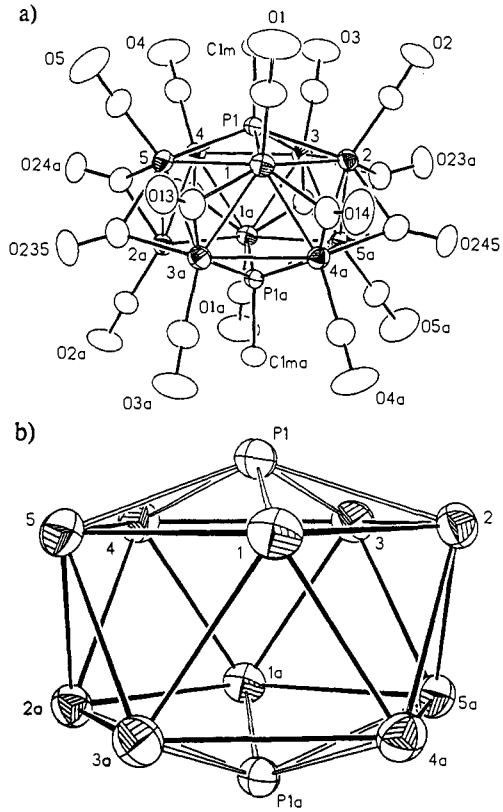

Figure 3. (a) Configuration of the $[Ni_{10}(PMe)_2(CO)_{18}]^{2-}$ dianion (**2**) in the $[PPh_3Me]^+$ salt (**2a**). This dianion, which possesses ten terminal, four doubly bridging, and four triply bridging carbonyl ligands, has crystallographic C_i-$\bar{1}$ site symmetry and closely conforms to C_{2h}-$2/m$ symmetry. The anisotropic atomic thermal ellipsoids are at the 35% probability level. (b) The noncentered 1,2-disubstituted $Ni_{10}P_2$ icosahedral cage of **2**. The pseudo-D_{5d} symmetry of the $Ni_{10}P_2$ cage is reduced to C_{2h}-$2/m$ upon inclusion of the doubly and triply bridging carbonyl ligands which markedly influence the individual bond lengths of both the intrapentagonal and the interpentagonal Ni–Ni distances. The pseudo-mirror plane contains Ni(1), Ni(1a), P(1), and P(1a).

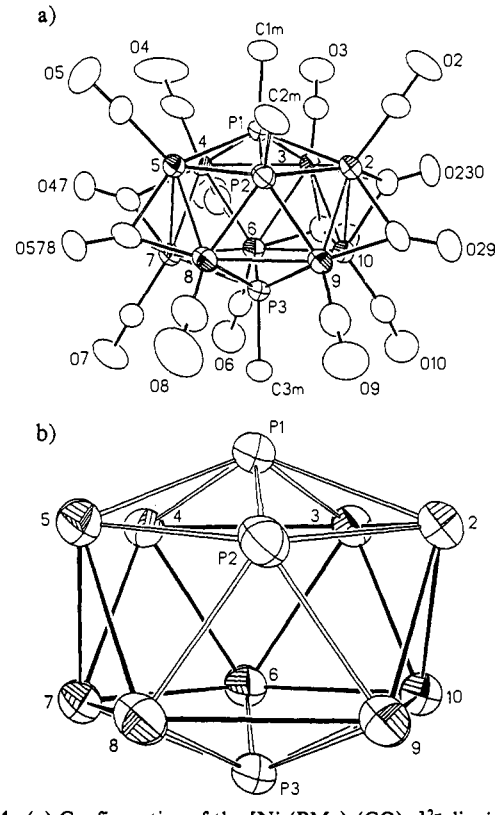

Figure 4. (a) Configuration of the $[Ni_9(PMe)_3(CO)_{15}]^{2-}$ dianion (**3**) in the $[PPh_3Me]^+$ salt (**3a**). This dianion of crystallographic C_1-1 site symmetry approximately conforms to C_s-m symmetry with nine terminal and six bridging carbonyl ligands. The arbitrary criterion that Ni–CO(bridging) distances greater than 2.5 Å represent nonbonding (instead of semibridging) carbonyl interactions results in the CO(29), CO(46), and CO(47) ligands being classified as doubly bridging and the CO(578), CO(230), and CO(360) ligands as triply bridging. The anisotropic atomic thermal ellipsoids are at the 35% probability level. (b) The noncentered 1,2,12-trisubstituted Ni_9P_3 icosahedral cage of **3** in **3a** which has a pseudo-mirror plane passing through Ni(6) and the three phosphorus atoms.

in THF and acetone. An infrared spectrum of **4a** in THF exhibited a strong terminal band at 1960 cm^{-1} and a bridging carbonyl band at 1755 (mw) cm^{-1}. A cyclic voltammogram of **4** in THF showed a quasireversible oxidation wave at −0.34 V and an irreversible reduction at ca. −1.00 V.

A ^1H NMR spectrum of **4a** at 22 °C showed a single resonance at δ 1.75 which was assigned to the methyl protons. All other proton signals were due to the solvent and counterion. A $^{31}P\{^1H\}$ NMR spectrum of **3** exhibited a singlet at δ −41.1. The ^{31}P resonance at δ 22.6 was assigned to the $[PPh_3Me]^+$ counterion.

X-ray Crystallographic Determinations and Refinements. (a) General Procedures. Each crystal was mounted under an argon atmosphere inside a Lindemann glass capillary which was then hermetically sealed. Intensity data were obtained with graphite-monochromated Mo Kα radiation on either a refurbished Siemens $P\bar{1}$ or Siemens $P3/F$ diffractometer. Unit-cell determinations were based upon a minimum of 20 well-centered reflections; axial photographs were taken to verify lattice lengths and unit cell symmetry. The intensities of standard reflections showed no significant variations (except for **5a**) during the entire collection of data. Absorption corrections[36-38] were applied to each data set. Crystallographic computations were carried out with SHELXTL PLUS[36] on VAX computers. Initial positions for Ni and P atoms were found by direct methods (**2a, 3a, 4a, 5a, 6a**) or by interpretation of the Patterson map (**3b**). The other non-hydrogen atoms were obtained from successive Fourier difference maps coupled with isotropic least-squares refinement. Hydrogen atoms were modeled in idealized positions with fixed isotropic thermal parameters. Final Fourier difference maps exhibited no unusual features. Crystal data, data-collection parameters, and least-squares refinement parameters are given in Table I. Tables of the positional and anisotropic thermal parameters for the non-hydrogen atoms, selected interatomic distances and bond angles, and idealized atomic parameters for the hydrogen atoms are available as supplementary material.

(b) $[PPh_3Me]^+_2[Ni_{10}(PMe)_2(CO)_{18}]^{2-}$ (2a). Crystals of **2a** were obtained by a layering of cyclohexane over a THF solution. X-ray data were collected at ambient temperature from a plate-shaped crystal (of approximate dimensions 0.7 × 0.2 × 0.4 mm) which was determined to be triclinic. A statistical analysis of the data indicated the probable space group to be $P\bar{1}$. Figure 3 displays the configurations of the dianion (**2**) and its $Ni_{10}P_2$ icosahedral cage in the $[PPh_3Me]^+$ salt (**2a**).

(c) $[PPh_3Me]^+_2[Ni_9(PMe)_3(CO)_{15}]^{2-}$ (3a). Crystals of **3a** were obtained by a layering of cyclohexane over a THF solution. X-ray data were acquired at ambient temperature from a plate-shaped crystal (of approximate dimensions 0.1 × 0.3 × 0.6 mm) which was found to be triclinic. A statistical analysis of the data indicated the probable space group to be $P\bar{1}$. Figure 4 shows the configurations of the dianion (3) and its Ni_9P_3 icosahedral cage in the $[PPh_3Me]^+$ salt (**3a**).

(d) $[NMe_4]^+_2[Ni_9(PMe)_3(CO)_{15}]^{2-}\cdot{}^7/_6\,C_6H_{12}$ (3b). Crystals of **3b** were grown by a layering of cyclohexane over a THF solution. A needle-shaped crystal (of approximate dimensions 0.7 × 0.3 × 0.3 mm) was determined to be rhombohedral; diffraction data which conformed to C_{3i}-$\bar{3}$ Laue symmetry were collected at −80 °C for the independent $\bar{h}kl$ octant of the triply primitive hexagonal setting of the rhombohedral unit cell. A statistical analysis of the data indicated a centrosymmetric distribution in accordance with the probable space group being $R\bar{3}$ with Z = 18 for the hexagonal unit cell. Figure 5 gives the configurations of the dianion (**3**) and its Ni_9P_3 icosahedral cage in the cyclohexane-solvated $[NMe_4]^+$ salt (**3b**).

(e) $[Na(C_4H_8O)_4]^+[Ni_9(PMe)_3(CO)_{14}(\mu_2\text{-}PMe_2)]^-$ (5a). Crystals of **5a** were obtained by a layering of cyclohexane over a THF solution.

(36) SHELXTL-PLUS, Siemens Analytical X-Ray Instruments, Inc.
(37) Empirical absorption corrections based upon ψ-scan measurements at different azimuthal angles were calculated with the XEMP program (SHELXTL-PLUS).
(38) (a) Alcock, N. W. *Crystallographic Computing*; Ottowa Summer School, 1969. (b) DeMeulenaer, J.; Tompa, H. *Acta Crystallogr.* **1965**, *19*, 1014–1018.

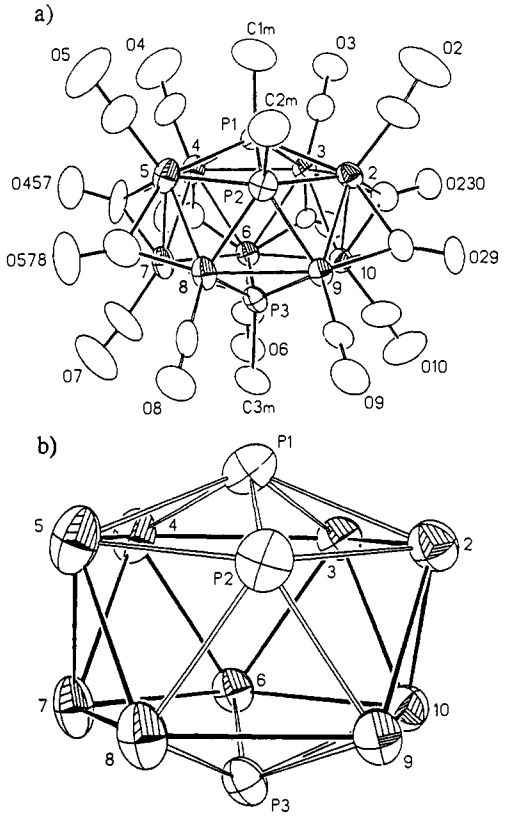

Figure 5. (a) Configuration of the $[Ni_9(PMe)_3(CO)_{15}]^{2-}$ dianion (**3**) in the $[NMe_4]^+$ salt (**3b**). Its solid-state architecture of crystallographic C_1-1 site symmetry and pseudo-C_s symmetry has nine terminal and six bridging carbonyl ligands. The arbitrary criterion that Ni–CO(bridging) distances greater than 2.5 Å represent nonbonding (instead of semibridging) carbonyl interactions results in the CO(29), CO(46), and CO(36) ligands being classified as doubly bridging and the CO(578), CO(230), and CO(457) ligands as triply bridging. Although the overall disposition of the six bridging carbonyl ligands in **3** is the same in the two salts (**3a** and **3b**), the markedly different Ni–CO(bridging) distances observed for two of the six bridging carbonyl ligands emphasize that the modes of asymmetric bridging carbonyl interactions with the Ni_9P_3 cage are strongly influenced by solid-state packing forces. (b) The noncentered 1,2,12-trisubstituted Ni_9P_3 icosahedral cage of **3** in **3b**; its geometry is nearly identical with that in **3a**.

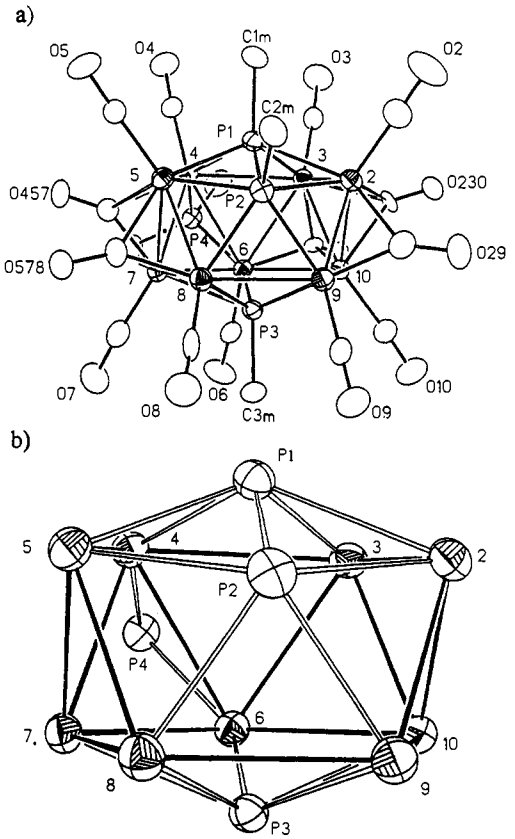

Figure 6. (a) Configuration of the $[Ni_9(PMe)_3(CO)_{14}(\mu_2\text{-}PMe_2)]^-$ monoanion (**5**) in the $[Na(C_4H_8O)_4]^+$ salt (**5a**). This monoanion of C_1-1 symmetry has an exocyclic dimethylphosphido bridging ligand along with nine terminal, one doubly bridging, and four triply bridging carbonyl ligands. The triply bridging carbonyl O(230) and O(578) atoms are linked by strong ion-pair interactions with octahedrally-coordinated $[Na(THF)_4]^+$ cations. The structural similarity and electronic equivalence of **5** with **3** is based upon the three-electron-donating dimethylphosphido bridging ligand in **5** being formally substituted for one doubly bridging carbonyl ligand and one negative charge in **3**. The anisotropic atomic thermal ellipsoids are drawn at the 35% probability level. (b) The noncentered 1,2,12-trisubstituted Ni_9P_3 icosahedral cage of **5** and the exocyclic dimethylphosphido phosphorus atom, P(4). This 1,2,12-trisubstituted icosahedral cage of **5** in **5a** closely conforms to those of **3** in **3b** except for a notable increase by 0.12 Å in the Ni(4)–Ni(6) distance due to the replacement of the symmetrical doubly bridging CO ligand spanning the Ni(4)–Ni(6) edge by the symmetrical doubly bridging PMe_2 ligand.

X-ray data were acquired at −60 °C from a block-shaped crystal (of approximate dimensions 0.2 × 0.4 × 0.7 mm) which was found to be triclinic. A linear correction of the intensities was made on the basis of the three standard reflections which displayed an average decay of 18% during data collection. A statistical analysis of the data indicated the probable space group to be $P\bar{1}$. Figure 6 displays the configurations of the monoanion (**5**) and its Ni_9P_3 icosahedral cage in the THF-solvated Na^+ salt (**5a**).

(f) $[PPh_3Me]^+_2[Ni_8(PMe)_4(CO)_{12}]^{2-}\cdot C_6H_{12}$ (4a). Crystals of **4a** were obtained by a layering of cyclohexane over a THF solution of **4a**. X-ray data were acquired at ambient temperature from a wedge-shaped crystal (of approximate dimensions 0.2 × 0.4 × 0.7 mm) which was found to be triclinic. A statistical analysis of the data indicated the probable space group to be $P\bar{1}$. The configurations of the dianion (**4**) and its Ni_8P_4 icosahedral cage in the cyclohexane-solvated $[PPh_3Me]^+$ salt (**4a**) are presented in Figure 7.

(g) $[PPh_3Me]^+_2[Ni_{10}(\mu_5\text{-}PMe)_2(\mu_4\text{-}PMe)_5(CO)_{10}]^{2-}\cdot C_4H_8O$ (6a). Crystals of **6a** were obtained by a layering of diisopropyl ether over a THF solution. X-ray data were collected at −80 °C from a plate-shaped crystal (of approximate dimensions 0.5 × 0.3 × 0.1 mm) which was determined to be orthorhombic. Observed systematic absences of $\{hkl\}$ for $h + k$ odd and $\{h0l\}$ for l odd indicated the probable space group to be $C2cm$ (a nonstandard setting of $Ama2$), $Cmc2_1$, or $Cmcm$. A statistical analysis of the data indicated a centrosymmetric $|E^2 - 1|$ distribution, thereby pointing to the centrosymmetric space group $Cmcm$. However, solution and refinement under the centrosymmetric $Cmcm$ space group resulted in the $[PPh_3Me]^+$ cation being disordered across the mirror plane normal to the c direction. A separate structural determination and analogous refinement under the noncentrosymmetric space group $Cmc2_1$ suggested an ordered crystal structure with lower values for both $R_1(F)$ (5.93% vs 6.86%) and $R_2(F)$ (7.60% vs 8.28%). The particular choice under $Cmc2_1$ of the polar axial c direction was indicated from an η-type refinement.[36,39] The highest positive residual peak found on a final Fourier difference map was located at the position expected for the crystal-disordered phosphorus atom; its occurrence may likely be a consequence of the pseudocentrosymmetric crystal structure due to the dianion (**6**).

Nevertheless, the configuration of $[Ni_{10}(\mu_5\text{-}PMe)_2(\mu_4\text{-}PMe)_5(CO)_{10}]^{2-}$ (**6**), presented in Figure 8, and its molecular parameters are based upon the structural refinement under $Cmcm$ symmetry which constrains the "average" structure of the dianion to crystallographic C_{2v}-$m2m$ site symmetry. Although the mean interatomic distances and bond angles of **6** obtained from the two separate least-squares refinements are virtually identical, the individual values based upon the $Cmcm$ refinement are more consistent with much lower esds (by $^1/_2$ to $^1/_4$) than those based upon the $Cmc2_1$ refinement. In addition, the sizes and shapes of the atomic thermal ellipsoids based upon the centrosymmetric $Cmcm$ refinement are reasonable. This problem in choosing between an ordered crystal structure in a noncentrosymmetric space group and a possibly disordered crystal structure in the corresponding centrosymmetric space group (in this case involving only the configuration of the $[PPh_3Me]^+$

(39) Rogers, D. *Acta Crystallogr.* **1981**, *A37*, 734–741.

Table I. Crystal, Data-Collection, and Refinement Parameters for $[PPh_3Me]^+_2[Ni_{10}(PMe)_2(CO)_{18}]^{2-}$ (**2a**), $[PPh_3Me]^+_2[Ni_9(PMe)_3(CO)_{15}]^{2-}$ (**3a**), $[NMe_4]^+_2[Ni_9(PMe)_3(CO)_{15}]^{2-}\cdot{}^7/_6(C_6H_{12})$ (**3b**), $[PPh_3Me]^+_2[Ni_8(PMe)_4(CO)_{12}]^{2-}\cdot(C_6H_{12})$ (**4a**), $[Na(C_4H_8O)_4]^+[Ni_9(PMe)_3(PMe_2)(CO)_{14}]^-$ (**5a**), and $[PPh_3Me]^+_2[Ni_{10}(PMe)_7(CO)_{10}]^{2-}\cdot(C_4H_8O)$ (**6a**)

	2a	3a	3b	4a	5a	6a
temp (°C)	21	21	−80	21	−60	−80
formula	$C_{58}H_{42}O_{18}P_4Ni_{10}$	$C_{56}H_{45}O_{15}P_5Ni_9$	$C_{33}H_{47}N_2O_{15}P_3Ni_9$	$C_{60}H_{60}O_{12}P_6Ni_8$	$C_{35}H_{47}O_{18}NaP_4Ni_9$	$C_{59}H_{65}O_{11}P_9Ni_{10}$
formula weight (g/mol)	1737.9	1641.2	1333.0	1628.6	1430.8	1815.9
$F(000)$	874	1656	12168	830	1448	3688
crystal system	triclinic	triclinic	rhombohedral	triclinic	triclinic	orthorhombic
a (Å)	10.351 (3)	10.366 (3)	41.91 (1)	9.106 (2)	10.335 (2)	26.293 (13)
b (Å)	12.294 (4)	13.682 (4)	41.91 (1)	13.472 (6)	13.799 (3)	17.869 (7)
c (Å)	12.801 (4)	22.089 (6)	14.289 (4)	14.173 (7)	19.189 (4)	15.673 (4)
α (deg)	86.97 (2)	86.28 (2)	90	109.83 (4)	88.43 (2)	90
β (deg)	76.81 (2)	84.80 (2)	90	99.14 (7)	87.54 (2)	90
γ (deg)	87.89 (2)	86.63 (2)	120	93.38 (14)	70.40 (2)	90
V (Å^3)	1583.2 (7)	3109.0 (15)	21737.8	1602.9 (10)	2575.2 (10)	7363.3 (50)
space group	$P\bar{1}$	$P\bar{1}$	$R\bar{3}$	$P\bar{1}$	$P\bar{1}$	$Cmcm$
Z	1	2	18	1	2	4
d (calcd) (g/cm^3)	1.823	1.753	1.833	1.687	1.845	1.638
μ (mm^{-1})	3.07	2.85	3.59	2.50	3.41	2.74
scan mode	ω	ω	θ–2θ	ω	θ–2θ	Wyckoff ω
2θ limits (deg)	3.5–52	3.5–45	4–45	3.5–55	3.5–48	3.5–45
scan speed (deg/min)	variable (3–30)	variable (3–30)	variable (4–30)	variable (3–30)	variable (3–30)	variable (3–30)
no. of check refl/freq	3/47	3/47	3/47	3/47	3/47	3/47
no. of indep data ($\|F\| > 3\sigma(F)$)	3873	5313	4507	5755	2198	1901
no. of parameters refined	409	514	425	281	230	183
data/parameter ratio	9.47/1	10.5/1	10.6/1	20.5/1	9.56/1	10.4/1
$R_1(F)$[a]	4.15	6.54	7.58	5.24	8.17	6.87
$R_2(F)$[a]	5.61	7.00	8.98	6.76	8.46	8.29
goodness-of-fit (GOF)	1.041	1.399	1.849	1.491	1.541	1.670

[a] $R_1(F) = [\sum||F_o| - |F_c||/\sum|F_o|] \times 100$ and $R_2(F) = [\sum w_i||F_o| - |F_c||^2/\sum w_i|F_o|^2]^{1/2} \times 100$.

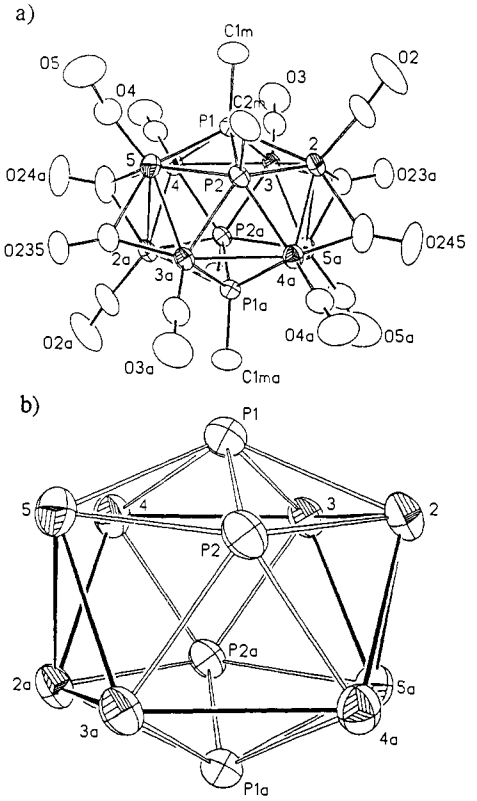

Figure 7. (a) Configuration of the $[Ni_8(PMe)_4(CO)_{12}]^{2-}$ dianion (**4**) in the $[PPh_3Me]^+$ salt (**4a**). This dianion of crystallographic C_i-$\bar{1}$ site symmetry approximately conforms to D_{2h}-mmm symmetry with eight terminal carbonyl and four triply bridging carbonyl ligands. The anisotropic atomic thermal ellipsoids are drawn at the 35% probability level. (b) The noncentered icosahedral 1,2,9,12-tetrasubstituted Ni_8P_4 cage of **4** which has one mirror plane containing the four phosphorus atoms and two other perpendicular mirror planes each containing four nickel atoms.

counterion which is not of interest to this work) has been encountered often in other structures; the common practice in choosing the centrosymmetric space group to describe more correctly the crystal structure is discussed elsewhere.[40]

Results and Discussion

Structural Features of $[Ni_{10}(PMe)_2(CO)_{18}]^{2-}$ (2). The 1,2-disubstituted icosahedron of **2** in each of the three salts (**2a**, **2b**, **2c**) with the $[PPh_3Me]^+$, $[Ph_3PNPPh_3]^+$, and $[NMe_4]^+$ counterions, respectively, is remarkably similar, as evidenced by analogous variations and close agreements of the corresponding individual distances as well as by the average icosahedral center-to-cage atom distances and mean Ni–P and Ni–Ni distances being within 0.01 Å. Likewise, the arrangements of the 18 carbonyl ligands about the $Ni_{10}P_2$ icosahedron are the same in each salt. Hence, the different interionic packing forces in these three salts do not significantly change either the configuration or dimensions of **2**. Since the X-ray diffraction study of $[PPh_3Me]^+_2[Ni_{10}(PMe)_2(CO)_{18}]^{2-}$ (**2a**) gave the most precise structure of **2**, as indicated directly by the smallest bond length esds and indirectly by the lower discrepancy values and the relatively high data-to-parameter ratio, the crystallographic data for only this salt are utilized in a description of the structural features of **2** and in a comparative analysis with the other icosahedral dianions (vide infra).

The centrosymmetric, 1,12-disubstituted icosahedral cage of pseudo-D_{5d} symmetry can be viewed as a pentagonal antiprism of 10 nickel atoms with two capping methylphosphinidene phosphorus atoms through which the principal 5-fold axis passes. The pseudo-D_{5d} symmetry of the $Ni_{10}P_2$ cage is reduced to C_{2h}-$2/m$ upon inclusion of the doubly and triply bridging carbonyl ligands which markedly influence the individual bond lengths of both the intrapentagonal and the interpentagonal Ni–Ni distances. The configuration of **2** is analogous to that of the centrosymmetric $[Ni_{10}(ER)_2(CO)_{18}]^{2-}$ homologues (E = As, R = Me;[19] E = Sb, R = Ph[22]). A geometrical comparison of these $Ni_{10}E_2$ dianions (E = P, As, Sb) has been presented elsewhere.[22]

Structural Features of $[Ni_9(PMe)_3(CO)_{15}]^{2-}$ (3) and $[Ni_9(PMe)_3(CO)_{14}(\mu_2\text{-}PMe_2)]^-$ (5). The 1,2,12-trisubstituted Ni_9P_3 icosahedral cages of **3** in the $[PPh_3Me]^+$ and cyclohexane-solvated $[NMe_4]^+$ salts (**3a** and **3b**) and of **5** in the $[Na(THF)_4]^+$ salt (**5a**) are geometrically analogous. The corresponding mean distances

(40) (a) Ziller, J. W.; Rheingold, A. L. X-Ray Crystallography. In Drago, R. S. *Physical Methods for Chemists*, 2nd ed., Harcourt, Brace, Jovanovich Publishers: Orlando, FL, 1992; Chapter 17. (b) Marsh, R. E.; Herbstein, F. H. *Acta Crystallogr.* **1988**, *B44*, 77–88 and references therein.

Table II. Mean Distances (Å) for Three Electronically Equivalent Members of the $[Ni_{12-x}(PMe)_x(CO)_{24-3x}]^{2-}$ Series (x = 2 (**2**), 3 (**3**), 4 (**4**)) and $[Ni_9(PMe)_3(CO)_{14}(\mu_2\text{-}PMe_2)]^-$ (**5**) as the $[PPh_3Me]^+$ Salts Containing Noncentered Icosahedral 1,12-$Ni_{10}P_2$, 1,2,12-Ni_9P_3, and 1,2,9,12-Ni_8P_4 Cages

cluster cage	site symmetry	pseudosymmetry	Ni–Ni distances	Ni–P distances	P–P distances	center–Ni distances	center–P distances
$Ni_{10}P_2$ (**2**)	C_i-$\bar{1}$	D_{5d}	2.55 [20][a]	2.35 [10]	— [0]	2.46 [10]	1.79 [2]
Ni_9P_3 (**3**)	C_1-1	C_s	2.55 [16]	2.33 [13]	2.27 [1]	2.42 [9]	1.97 [3]
Ni_9P_3 (**5**)	C_1-1	C_s	2.55 [16]	2.32 [13]	2.26 [1]	2.42 [9]	1.97 [3]
Ni_8P_4 (**4**)	C_i-$\bar{1}$	D_{2h}	2.53 [12]	2.31 [16]	2.28 [2]	2.39 [8]	2.03 [4]

[a] The number enclosed within the square brackets designates the number of equivalent edge connectivities given by the mean value.

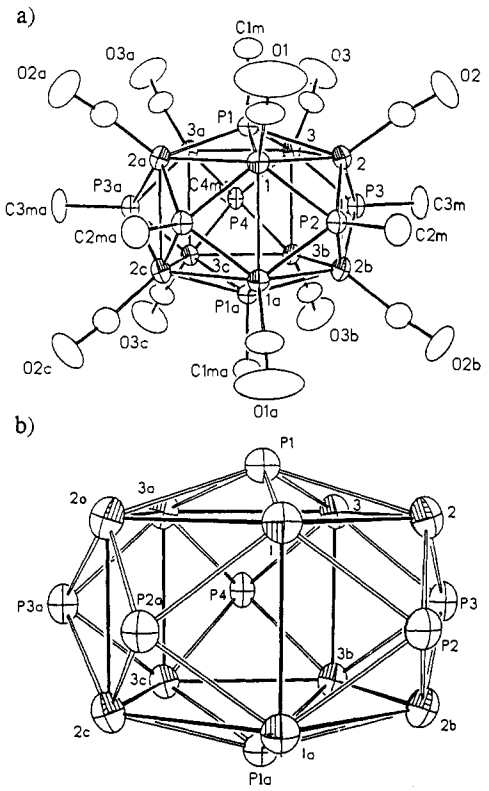

Figure 8. (a) Configuration of the $[Ni_{10}(\mu_5\text{-}PMe)_2(\mu_4\text{-}PMe)_5(CO)_{10}]^{2-}$ dianion (**6**) in the THF-solvated $[PPh_3Me]^+$ salt (**6a**). This dianion of crystallographic C_{2v}-*m*2*m* site symmetry under *Cmcm* symmetry consists of a pentagonal prismatic Ni_{10} kernel capped on all seven faces by methylphosphinidene ligands; a terminal carbonyl ligand is coordinated to each nickel atom. One crystallographic mirror plane perpendicular to the *a* axis passes through the five tetracapping phosphorus and their attached methyl carbon atoms, while the other mirror plane perpendicular to the *c* axis passes through Ni(1), Ni(1a), P(1), P(1a), P(4), and their attached ligands; the 2_b axis along the line of intersection of the two perpendicular mirror planes passes through P(4) and C(4m). The heptacapped pentagonal prismatic $Ni_{10}P_7$ core of pseudo-D_{5h} symmetry is encompassed by a semiregular 17-vertex polyhedron formed from 10 carbonyl oxygen atoms and seven P-attached methyl carbon atoms. The polyhedral ligand arrangement may be considered as a 5-layer (1:5:5:5:1) deltahedron composed of 30 triangular faces with the analogous D_{5h} symmetry. (b) The noncentered omnicapped pentagonal prismatic Ni_{10} cage of **6** with the seven capping methylphosphinidene phosphorus atoms. To our knowledge, there is no previous example of this 17-vertex D_{5h} polyhedron.

in the three Ni_9P_3 cages are all within 0.01 Å of one another except for one difference of 0.02 Å. Each noncentrosymmetric Ni_9P_3 cage has a pseudo-mirror plane passing through one nickel and the three phosphorus atoms.

The Ni_9P_3 cages of **3** in **3a** and **3b** are surrounded by 15 similarly disposed carbonyl ligands, of which nine terminal CO ligands are each coordinated to a different nickel atom and six bridging CO ligands are connected between the P-capped Ni_4P and Ni_5 pentagons. The formal interconversion of **3** into **5** involves the replacement of the symmetrical doubly bridging CO together with one negative charge by a symmetrical doubly bridging PMe_2 ligand. The cage of **5** closely conforms to those of **3** in **3a** and **3b** except for an increase by 0.12 Å in the Ni(4)–Ni(6) bond length bridged by the PMe_2 ligand.

The modes of linkage of two of the five common bridging carbonyl ligands to the Ni_9P_3 cages markedly vary among the three salts, as evidenced by large differences in the Ni–CO(bridging) bond lengths for the CO(457) and CO(360) ligands. If Ni–CO(bridging) distances greater than 2.50 Å are arbitrarily classified as nonbonding instead of weakly bonding (in accordance with highly asymmetrical triply bridging CO ligands), it follows that the CO(457) ligand of **3** is doubly bridging in **3a** and triply bridging in **3b** whereas the CO(360) ligand of **3** is triply bridging in **3a** but doubly bridging in **3b**. It is noteworthy that both of these two CO ligands are triply bridging in **5a**. In contrast, the CO(29) ligand is doubly bridging and the CO(578) and CO(230) ligands are triply bridging in all three salts. The different bridging carbonyl distributions found in **3a** and **3b** are attributed to dissimilar packing interactions. Despite these distinct variations in certain Ni–CO(bridging) distances, the overall configuration (including the CO ligands) of **3** in each of its two salts also conforms approximately to C_s-*m* symmetry. This mirror plane symmetry is destroyed in **5** by inclusion of the μ_2-PMe_2 ligand. The overall configuration of **3** is analogous to that previously found[19] for the $[Ni_9(AsPh)_3(CO)_{15}]^{2-}$ dianion in the THF-solvated $[NMe_4]^+$ salt.

Specific ion-pair interactions are observed in the $[Na(THF)_4]^+$ salt (**5a**) of **5**. This monoanion (**5**) was unexpectedly isolated via column chromatography as the $[Na(THF)_4]^+$ salt in very small yield (<3%) from one reaction of $[Ni_6(CO)_{12}]^{2-}$ (**1**) with $MePCl_2$. The structural determination of **5a** shows the existence of tight-ion pairing between the $[Na(THF)_4]^+$ cation and triply bridging carbonyl oxygen atom from each of the two translation-related monoanions. The central Na^+ ion thereby possesses an octahedral oxygen environment with two *trans* carbonyl oxygen atoms at Na^+–O distances of 2.489 (9) and 2.778 (9) Å and four THF oxygen atoms at Na^+–O distances of 2.274 (13), 2.281 (14), 2.307 (14), and 2.312 (13) Å.

Structural Features of $[Ni_8(PMe)_4(CO)_{12}]^{2-}$ (4). This centrosymmetric 1,2,9,12-tetrasubstituted Ni_8P_4 icosahedral cage of pseudo-D_{2h}-*mmm* symmetry has one mirror plane containing the four phosphorus atoms and two other perpendicular mirror planes each containing four nickel atoms. The 2-fold axis lying on the tetraphosphorus mirror plane passes through the midpoints of the two bonding pairs of phosphorus atoms, while each of the other two perpendicular 2-fold axes passes through the midpoints of the opposite bonding pairs of four nickel atoms. Each of the eight nickel atoms has a terminal carbonyl ligand; the other four carbonyl ligands are asymmetrically triply bridging.

Structural Comparison of $[Ni_{10}(PMe)_2(CO)_{18}]^{2-}$ (2), $[Ni_9(PMe)_3(CO)_{15}]^{2-}$ (3), and $[Ni_8(PMe)_4(CO)_{12}]^{2-}$ (4). (a) General Comment. A comparative geometrical examination of the $Ni_{12-x}P_x$ icosahedral cages of the three members in this homologous $[Ni_{12-x}(PMe)_x(CO)_{24-3x}]^{2-}$ series (x = 2, 3, 4) reveals distinct geometrical consequences resulting from the sequential substitution of two smaller isolobal PMe fragments for two $Ni(CO)_3$ fragments.

(b) Sizes, Shapes, and Edge-Connectivities of the $Ni_{12-x}P_x$ Icosahedral Cages. An inspection of the icosahedral center (I. C.)-to-cage atom distances in Table II discloses that the shape of the $Ni_{12-x}P_x$ cage greatly changes from a squashed cylindrical-type architecture for the centrosymmetric 1,12-$Ni_{10}P_2$ cage in **2** toward more spherical-like icosahedral architectures for both the noncentrosymmetric 1,2,12-Ni_9P_3 cage in **3** and centrosym-

Table III. Comparison of Corresponding Mean Edge Connectivities (Å) for the $Ni_{12-x}P_x$ Icosahedral Cages in the Homologous $[Ni_{12-x}(PMe)_x(CO)_{24-3x}]^{2-}$ Dianions (x = 2 (2), 3 (3), 4 (4)) with $[PPh_3Me]^+$ Counterions (2a, 3a, 4a)

edge connectivities	$Ni_{10}P_2$ cage in 2a	Ni_9P_3 cage in 3a	Ni_8P_4 cage in 4a
Ni–Ni(Ni,Ni)[a]	2.49 [10][b]	2.52 [6][b]	2.55 [2][b]
Ni–Ni(Ni,P)	2.62 [10]	2.57 [9]	2.52 [8]
Ni–Ni(P,P)	— [0]	2.55 [1]	2.55 [2]
Ni–P(Ni,Ni)	2.35 [10]	2.32 [9]	2.29 [8]
Ni–P(Ni,P)	— [0]	2.34 [4]	2.32 [8]
P–P(Ni,Ni)	— [0]	2.27 [1]	2.28 [2]

[a] The atoms within the parentheses bridge the given connectivity. [b] The number enclosed within the square brackets designates the number of equivalent edge connectivities given by the mean value.

metric 1,2,9,12-Ni_8P_4 cage in 4; this geometrical change is evidenced by the smaller difference between the decreasing mean I.C.–Ni distance and increasing mean I.C.–P distance on going from the pseudo-D_{5d} $Ni_{10}P_2$ cage (2.46 vs 1.79 Å) to the pseudo-C_s Ni_9P_3 cage (2.42 vs 1.97 Å) and then to the pseudo-D_{2h} Ni_8P_4 cage (2.39 vs 2.03 Å). It also is apparent that the cavity sizes for the empty $Ni_{12-x}P_x$ cages of 2, 3, and 4 decrease as phosphorus substitution increases due to the greater number of relatively shorter Ni–P bonding connectivities and correspondingly smaller number of longer Ni–Ni bonding connectivities. This cage-size trend is also evident from an examination of Table II which shows that the mean Ni–Ni edge-connectivities in a given $Ni_{12-x}P_x$ cage are 0.2 Å longer than the mean Ni–P edge-connectivities which in turn are somewhat longer than the mean P–P edge-connectivities (viz., ca. 0.06 Å longer in 3 and ca. 0.03 Å longer in 4).

In order to provide a comparison of the different types of Ni–Ni and Ni–P edge-connectivities for these three homologous $Ni_{12-x}P_x$ icosahedral (x = 2, 3, 4) containing dissimilar vertex distributions of nickel and phosphorus atoms, the following designation of edge-connectivities is used. Since a 12-atom icosahedron is composed of 20 edge-fused triangles and 30 connective edges, each common edge between two atoms is commonly bridged by two atoms which form the other two apices of the two edge-fused triangles. For example, the two bridging atoms involved in a given Ni–Ni connectivity in the Ni_9P_3 icosahedral cage may be bridged by two Ni atoms, one Ni and one P atom, or two P atoms. In order to differentiate among these three different Ni–Ni connectivities, we propose the symbolism Ni–Ni(Ni,Ni), Ni–Ni(Ni,P), and Ni–Ni(P,P) to designate the two bridging atoms. This nomenclature is utilized in Table III which presents a comparison of the mean edge-connectivities for the three $Ni_{12-x}P_x$ icosahedral cages of the homologous 2, 3, and 4 dianions with $[PPh_3Me]^+$ counterions (2a, 3a, 4a).

Although the ranges of individual distances within given types of edge-connectivities may be quite large, the mean values exhibit small but distinct trends among the $Ni_{12-x}P_x$ cages of 2, 3, and 4 which depend upon the nature of the edge-connectivity. Whereas the mean Ni–Ni(Ni,Ni) connectivities *increase* by two 0.03-Å increments upon going from 2 to 3 to 4, the corresponding mean Ni–Ni(Ni,P) connectivities *decrease* by two 0.05-Å increments and the mean Ni–P(Ni,Ni) connectivities *decrease* by two 0.03-Å increments. In contrast, the mean Ni–Ni(P,P) connectivities are identical in 3 and 4.

These different trends indicate that the average Ni–Ni and Ni–P connectivities within a given cage are dependent on the ratio of Ni atoms to P atoms as well as on their vertex distribution. Noteworthy is the existence to date of only one particular geometrical cage isomer for 2, 3, and 4; the fact that in each isomer two PMe fragments are at opposite (trans) 1,12-vertices from each other strongly indicates that steric effects involving the polyhedral ligand arrangement (viz., in this case involving both the methyl substituents and carbonyl groups) play a prominent role in dictating the kind of geometrical isomer formed as well as its composition (vide infra).

(c) Ligand Polyhedral Arrangements. From a systematic geometrical analysis of a large number of binary transition metal carbonyl clusters, Johnson and Benfield[41] have emphasized that the distribution of terminal, doubly bridging, and/or triply bridging carbonyl ligands in a given cluster reflects the ligand polyhedral arrangement of the carbonyl oxygen atoms and the orientation of the metal core within the ligand polyhedron. They pointed out that the carbonyl oxygen polyhedron for a majority of these clusters may be rationalized in terms of a simple model which postulates that the carbonyl ligands pack in space so as to minimize nonbonded interactions.

In 2, 3, or 4 the $Ni_{12-x}P_x$ icosahedral cage may similarly be regarded as a central core encapsulated by a ligand polyhedron consisting of carbonyl oxygen atoms and phosphorus-attached methyl groups. In 2, the spatial disposition of the 18 oxygen atoms may be envisioned as approximately conforming to succcessive 5, 8, 5 rings of oxygen vertices which are oriented perpendicularly to the principal 5-fold axis of the pseudo-D_{5d} 1,12-$Ni_{10}P_2$ cage; the two 1,12 phosphorus-attached methyl carbon atoms cap the outer two centrosymmetrically-related oxygen pentagons. In contrast to the near-planarity of the oxygen pentagonal rings, the eight oxygen atoms within the inner ring greatly deviate from coplanarity in filling the ligand sphere. This 20-vertex ligand polyhedron, which possesses the pseudo-C_{2h} symmetry of the entire dianion, has 52 edge-connectivities which form 32 triangular and two square faces.

The 15 oxygen atoms surrounding the 1,2,12-Ni_9P_3 core of 3 in both 3a and 3b roughly form a pseudo-C_s 5, 6, 4 distribution of oxygen vertices along the line between the trans P atoms (i.e., the 1,12 positions); the third P-attached methyl carbon atom in 3 is spatially oriented in place of a triangular oxygen face in 2 originating from one terminal and two bridging oxygen atoms.

In 4, the 12 oxygen atoms form a single ring of eight oxygen vertices with two oxygen vertices above and below the ring. Due to the increased substitution, it is easier to view the overall ligand polyhedron of 12 oxygen and 4 carbon atoms as a 16-vertex polyhedron of pseudo-D_{2h} symmetry which may be described as a 4, 8, 4 ring distribution of vertices relative to the 2-fold axis passing through the midpoints of the two bonding pairs of phosphorus atoms. This 16-vertex ligand polyhedron in 4 is analogous to that shown[41] for the 16 carbonyl oxygen atoms encompassing the planar Re_4 core in the pseudo-D_{2h} $[Re_4(CO)_{16}]^{4-}$ tetraanion.[42]

The sequential replacement of three carbonyl oxygen atoms by one methyl carbon atom on going from 2 to 3 to 4 results in the occurrence of large distances between certain vertices in the 18-vertex ligand polyhedron of 3 and the 16-vertex ligand polyhedron of 4 due to the replacement of triangular oxygen faces originating from one terminal and two bridging carbonyl ligands by P-attached methyl carbon atoms. The oxygen vertices in 2, 3, and 4 remain in approximately the same polyhedral arrangement, although they are further spread out in space due to methyl ligands having a smaller cone angle than three carbonyl ligands.

This structural comparison provides clearcut evidence that the steric effects of the ligand polyhedra play a major role along with electronic effects in dictating not only the formation of the geometrical isomers found for the $Ni_{12-x}P_x$ icosahedra (x = 2, 3, 4) but also their sizes, shapes, and orientations within the ligand polyhedra.

Theoretical and Experimental Analyses of the $[Ni_{12-x}P_x(CO)_{24-3x}]^{2-}$ Series (x = 2, 3, 4) and Resulting Implications. (a) Qualitative Bonding Descriptions. According to the polyhedral skeletal electron-pair (PSEP) model,[43] a closo system should possess (n + 1) electron pairs for skeletal cluster bonding. The 12-vertex icosahedral cage should therefore have 13 skeletal

(41) (a) Benfield, R. E.; Johnson, B. F. G. *J. Chem. Soc., Dalton Trans.* **1980**, 1743–1767. (b) Johnson, B. F. G.; Benfield, R. E. In *Topics in Inorganic and Organometallic Stereochemistry*; Geoffroy, G., Ed.; John Wiley & Sons: New York, 1981; Vol. 12, pp 253–335. (c) Johnson, B. F. G.; Benfield, R. E. *J. Chem. Soc. Dalton Trans.* **1978**, 1554–1568. (d) Johnson, B. F. G. *J. Chem. Soc., Chem. Commun.* **1976**, 211–212.

(42) Churchill, M. R.; Bau, R. *Inorg. Chem.* **1968**, *7*, 2606–2614.

(43) (a) Wade, K. *J. Chem. Soc., Chem. Commun.* **1971**, 792–793. (b) Wade, K. *Electron Deficient Compounds*; Thomas Nelson and Sons, ltd.: London, 1971. (c) Wade, K. *Adv. Inorg. Chem. Radiochem.* **1976**, *18*, 1–66.

electron pairs involved in delocalized bonding. The PSEP model[43] assumes that only three internal valence orbitals at each atomic vertex are involved in skeletal cluster bonding; the expected electron-pair count of 13 for each of the $Ni_{12-x}P_x$ cages of **2**, **3**, and **4** results from each Ni(CO), PMe, and CO donating zero, two, and one skeletal electron pairs, respectively, with the remaining skeletal electron pair being provided by the −2 charge of the dianion.

Application of cluster valence electron-counting rules[44-46] to these $Ni_{12-x}P_x$ cages necessitates that each main-group phosphorus atom be counted as part of the core, in which case the electron-pair P–Me bond is included in the valence electron count. This gives rise to the observed number of cluster valence electrons (CVEs) being 150 for $[Ni_{10}(PMe)_2(CO)_{18}]^{2-}$ (**2**), 140 for $[Ni_9(PMe)_3(CO)_{15}]^{2-}$ (**3**), and 130 for $[Ni_8(PMe)_4(CO)_{12}]^{2-}$ (**4**). The electron counts are in agreement with each substitution of a $Ni(CO)_3$ fragment by an isolobal PMe fragment, decreasing the number of CVEs by 10 since the main group P atom does not have any d valence electrons.

The reverse substitution of each PMe fragment in **2**, **3**, or **4** by an electronically equivalent $Ni(CO)_3$ fragment results in the formation of the hypothetical $[Ni_{12}(CO)_{24}]^{2-}$ dianion with an all-metal icosahedral cage. Its 170 CVEs, which are equivalent to 13 skeletal electron pairs upon substraction of 144 external electrons belonging to the 72 non-skeletal external orbitals (i.e., 12 × 6) of the 12 transition metal cage atoms, are expectedly in accordance with the different electron counting models for a metal icosahedron. A prime question is whether such a $[Ni_{12}(CO)_{24}]^{2-}$ dianion can be isolated. From an extension of the Tolman cone-angle concept,[47] Mingos[48] proposed that an icosahedron composed of first-row transition metals should be able to accommodate as many as 25 carbonyl ligands around it periphery. However, we presume from steric considerations that the hypothetical $[Ni_{12}(CO)_{24}]^{2-}$ dianion would be unstable relative to decarbonylation with formation of the three-layer (3:6:3) hcp $[Ni_{12}(CO)_{21}H_{4-n}]^{n-}$ anions (n = 2, 3, 4).[49] The fact that reactions of **1** with the bulky Me_3CPCl_2 reagent yielded a variety of high-nuclearity nickel carbonyl–phosphinidene clusters[31] but did not produce a noncentered icosahedron further demonstrates the importance of steric effects arising from interligand nonbonding repulsions in dictating the number of permissible polyhedral arrangements of the carbonyl and substituents of the main-group ER fragments for a given Ni_yE_x core composition.

It is also of interest to speculate about the possibility of extending the homologous $[Ni_{12-x}(PR)_x(CO)_{24-3x}]^{2-}$ series to x = 5 and 6 which would result in the $[Ni_7(PR)_5(CO)_9]^{2-}$ and $[Ni_6(PR)_6(CO)_6]^{2-}$ dianions. While there appears to be no geometrical constraint which would preclude the existence of these hypothetical clusters, the resulting small number of π-acceptor CO ligands is presumably insufficient to stabilize such highly reduced cluster cores and may prevent their formation on grounds of chemical reactivity.

(b) Infrared Spectral Analysis. Solution infrared spectra (Figure 1) of **2**, **3**, and **4** are in accordance with their configurations as determined by the X-ray diffraction studies. The frequency of the single strong terminal carbonyl band in each spectrum decreases from 2010 cm^{-1} in **2** to 1985 cm^{-1} in **3** to 1960 cm^{-1} in **4**. This linear decrease in carbonyl frequency is ascribed to enhanced Ni(dπ)–CO(π^*) backbonding resulting from the electron-density surface charge of the $Ni_{12-x}P_x$ cage being largest for **4** (x = 4) and smallest for **2** (x = 2). This increased negative surface charge on going from **2** to **3** to **4** is attributed to the greater number of PMe fragments and correspondingly fewer $Ni(CO)_3$ fragments with π-acceptor CO ligands. The relatively strong bridging carbonyl band at 1830 (m) cm^{-1} in **2** also decreases to 1805 (mw) cm^{-1} in **3** and then to 1755 (mw) cm^{-1} in **4**. This trend is likewise consistent with greater charge removal from the more electron-rich $Ni_{12-x}P_x$ cage on going from **2** (x = 2) to **3** (x = 3) to **4** (x = 4).

(c) NMR Spectral Analysis. Room temperature $^{31}P\{^1H\}$ NMR solution spectra of $Ni_{10}P_2$ **2** and Ni_8P_4 **4** each exhibit a single phosphorus resonance in accordance with their solid-state structures which each contain chemically equivalent phosphorus atoms; hence, these spectra give no insight concerning possible cage fluxionality. However, a $^{31}\{^1H\}$ NMR solution spectrum of the Ni_9P_3 **3** at room temperature displays three well-resolved phosphorus signals with an ABX splitting pattern that is completely consistent with the solid-state 1,2,12-Ni_9P_3 cage geometry in **3**. The ABX splitting pattern of **3** remains virtually unchanged at 50 °C and the fact that no other signals arising from other isomers are observed provides evidence that **3** has a rigid-cage structure in solution and suggests that **2** and **4** also possess rigid-cage structures in solution.

The $^{31}P\{^1H\}$ NMR signals at δ 271.9 ppm for the $Ni_{10}P_2$ **2** and at δ −41.1 ppm for the Ni_8P_4 **4** are the lowest and highest field resonances, respectively, observed for the $[Ni_{12-x}(PMe)_x(CO)_{24-3x}]^{2-}$ series. The chemical shifts of the three $^{31}P\{^1H\}$ NMR signals for the Ni_9P_3 **3** at δ 195.4, −5.4, and −10.5 ppm are between the extreme resonances found for **2** and **4**. The δ 195.4 ppm X resonance of the ABX spectrum of **3** is assigned to the phosphorus atom at position 12 of the 1,2,12-Ni_9P_3 cage. This phosphorus atom is in a chemically analogous environment to those of the chemically equivalent phosphorus atoms in the 1,12-$Ni_{10}P_2$ cage of **2**; each of these phosphorus atoms in **2** has the same five Ni–P connectivities. The δ −5.4 ppm A and the δ −10.5 ppm B resonances of **3** are tentatively assigned to the phosphorus atoms at positions 1 and 2, respectively, in the 1,2,12-Ni_9P_3 icosahedron. These latter two nonequivalent phosphorus atoms are in chemically similar environments to those of the four chemically equivalent phosphorus atoms in the 1,2,9,12-Ni_8P_4 icosahedron of **4**; each of these phosphorus atoms has one P–P and four Ni–P connectivities. The coupling constants based upon these assignments are J_{AB} = 332.5 Hz > J_{AX} = 222.3 Hz > J_{BX} = −122.5 Hz. Interestingly, the two phosphorus atoms in the 1 and 12 positions of the 1,2,12-Ni_9P_3 cage are coupled more strongly than the two phosphorus atoms in the 2 and 12 positions. Strong coupling between the two phosphorus atoms in the 1 and 12 positions in these $Ni_{12-x}P_x$ cluster cages is also evidenced by the occurrence of virtual coupling observed via the ^1H NMR spectrum for the methyl protons by the two symmetry equivalent phosphorus atoms in the 1,12-$Ni_{10}P_2$ cage of **2**.

^{31}P chemical shifts of the $Ni_{12-x}P_x$ icosahedral clusters approach higher field with increased PMe substitution suggesting that the phosphorus atoms experience greater shielding effects. Since each PMe substitution into the cage results in the loss of one $Ni(CO)_3$, the smaller number of CO(π^*) acceptor ligands results in a larger electron density distributed over the cluster cage; thus, the much higher $^{31}P\{^1H\}$ NMR chemical shift in **4** may reflect greater shielding effects due to increased electron density.

Variable-temperature $^{13}C\{^1H\}$ NMR studies of **2**, **3**, and **4** as well as of related icosahedral $[Ni_{10}(ER)_2(CO)_{18}]^{2-}$ dianions (E = As, Sb) are in progress in order to probe the fluxional behavior

(44) (a) Mingos, D. M. P. *Nature (London), Phys. Sci.* **1972**, *236*, 99–102. (b) Mingos, D. M. P.; Forsyth, M. I. *J. Chem. Soc., Dalton Trans.* **1977**, 610–616. (c) Evans, D. G.; Mingos, D. M. P. *J. Organomet. Chem.* **1982**, *240*, 321–327. (d) Mingos, D. M. P. *J. Chem. Soc., Chem. Commun.* **1983**, 706–708. (e) Evans, D. G.; Mingos, D. M. P. *Organometallics* **1983**, *2*, 435–447. (f) Mingos, D. M. P. *Acc. Chem. Res.* **1984**, *17*, 311–319. (g) Mingos, D. M. P. *J. Organomet. Chem.* **1985**, *280*, 407–418, 419–428. (h) Mingos, D. M. P.; Zhenyang, L. *J. Chem. Soc., Dalton Trans.* **1988**, 1657–1664 and references therein. (i) Mingos, D. M. P.; May, A. P. In *The Chemistry of Metal Cluster Complexes*; Shriver, D. F., Kaesz, H. D., Adams, R. D., Eds.; VCH Publishers: New York, NY; Chapter 2, pp 11–119. (j) Mingos, D. M. P.; Wales, D. J. *Introduction to Cluster Chemistry*; Prentice Hall: Englewood Cliffs, NJ, 1990.

(45) Lauher, J. W. *J. Am. Chem. Soc.* **1978**, *100*, 5305–5315.

(46) (a) Teo, B. K.; Longoni, G.; Chung, F. R. K. *Inorg. Chem.* **1984**, *23*, 1257–1266. (b) Teo, B. K. *Inorg. Chem.* **1985**, *24*, 1627–1638.

(47) Tolman, C. A. *Chem. Rev.* **1977**, *77*, 313–348.

(48) Mingos, D. M. P. *Inorg. Chem.* **1982**, *21*, 464–466.

(49) (a) Broach, R. W.; Dahl, L. F.; Longoni, G.; Cavalieri, A.; Chini, P.; Schultz, A. J.; Williams, J. M. *Adv. Chem. Ser.* **1978**, *No. 167*, 93–110. (b) Chini, P.; Longoni, G.; Manassero, M.; Sansoni, M. *Abstracts of the Eighth Meeting of the Italian Association of Crystallography*; Ferrara, 1977; Communication 34. (c) Ceriotti, A.; Chini, P.; Pergola, R. D.; Longoni, G. *Inorg. Chem.* **1983**, *22*, 1595–1598. (d) Ceriotti, A.; Chini, P.; Pergola, R. D.; Longoni, G. *Inorg. Chem.* **1983**, *22*, 1595–1598. (d) Nagaki, D. A.; Dahl, L. F. Unpublished research, 1986.

Table IV. Mean Distances (Å) for the Electron-Precise $[Ni_{10}(\mu_5\text{-PMe})_2(\mu_4\text{-PMe})_5(CO)_{10}]^{2-}$ (6) and $Ni_8(\mu_4\text{-PPh})_6(CO)_8$ (7)

cluster cage	site symmetry	idealized cage symmetry	Ni–Ni distances	Ni–(μ_4-P) distances	Ni–(μ_5-P) distances	center–Ni distances	center–(μ_5-P) distances
$Ni_{10}P_7$ (6)	C_{2v}-$m2m$	D_{5h}	2.62 [15][a]	2.16 [20]	2.33 [10]	2.58 [10]	2.02 [10]
Ni_8P_6 (7)	C_i-$\bar{1}$	O_h	2.65 [12]	2.18 [24]	— [0]	2.29 [8]	— [0]

[a] The number enclosed within the square brackets designates the number of equivalent edge connectivities given by the mean value.

of the terminal and bridging carbonyl ligands.[50]

(d) Electrochemical Analysis. Cyclic voltammograms of **2a**, **3a**, and **4a** in THF solution do not exhibit any reversible reductions out to −1.5 V. The $[Ni_{10}(PMe)_2(CO)_{18}]^{2-}$ dianion (2) shows an irreversible wave at E_p = 0.75 V, which indicates that this cluster undergoes either a significant rearrangement or decomposition at this potential. Both the $[Ni_9(PMe)_3(CO)_{15}]^{2-}$ dianion (**3**) and the $[Ni_8(PMe)_4(CO)_{12}]^{2-}$ dianion (**4**) exhibit quasireversible oxidation waves at 0.30 and −0.34 V, respectively, suggesting less structural change and perhaps greater stabilities associated with the oxidized species. Attempts to characterize compounds resulting from chemical oxidations of **2**, **3** and **4** are currently under investigation; to date only oxidized clusters of **4** have been isolated. The more negative E_p values for the oxidation waves observed upon increased PMe substitution for $Ni(CO)_3$ fragments for the homologous $[Ni_{12-x}P_x(CO)_{24-3x}]^{2-}$ series indicate that it is easiest to oxidize **4** and hardest to oxidize **2**. These results suggest that **4** contains the most electron-rich cluster cage as a result of the smaller number of CO(π^*) acceptor ligands available to remove electron density from the cluster cage.

Structural-Bonding Analysis of $[Ni_{10}(\mu_5\text{-PMe})_2(\mu_4\text{-PMe})_5(CO)_{10}]^{2-}$ (6). The $Ni_{10}P_7$ core in **6** is best described as a completely bonding pentagonal prism of nickel atoms capped on the two pentagonal and five rectangular faces by phosphinidene PMe fragments. A terminal carbonyl ligand is coordinated to each of the 10 nickel atoms. Alternately, the $Ni_{10}P_7$ core may be viewed as two eclipsed P-capped Ni_5 pentagons linked by five interpentagonal Ni–Ni bonds and five face-capping μ_4-P atoms. Under *Cmcm* space group symmetry this dianion has crystallographically imposed C_{2v}-$m2m$ site symmetry, but its entire geometry closely conforms to D_{5h} symmetry.

Table IV presents selected interatomic distances which are averaged under pseudo-D_{5h} symmetry. A comparison of **6** with the closely related $Ni_8(\mu_4\text{-PPh})_6(CO)_8$ (**7**),[51] in which all six square faces of a completely bonding Ni_8 cube are capped by PPh fragments, reveals the following prominent features: (1) The mean Ni–Ni distance of 2.62 Å in **6** is analogous to the mean Ni–Ni distance of 2.65 Å in **7**. (2) The mean Ni–(μ_4-P) distance of 2.16 Å in **6** compares favorably with the mean Ni–(μ_4-P) distance of 2.18 Å in **7**. (3) In **6**, the mean value for the Ni–(μ_5-P) distances is 0.17 Å longer than that for the Ni–(μ_4-P) distances. This increase in the average Ni–P(capping) distance for the two P(pentacapping) atoms is expected for the five associated edges of a degree five P vertex versus the four edges of a degree four P vertex. (4) The infrared terminal carbonyl frequency of 1990 cm^{-1} for **6** in THF is lower than that of 2020 cm^{-1} for **7** in CS_2; this 30 cm^{-1} frequency difference is readily attributed to enhanced Ni(dπ)–CO(π^*) backbonding in the dianion (**6**) relative to that in the neutral **7**.

The dianion (**6**) is the first example of a cluster with a completely bonding heptacapped pentagonal prismatic core. Consideration of the pentagonal nickel prism as the basic core unit gives rise to an observed electron count of 150 CVEs. Subtraction of 120 external electrons, which occupy the 60 nonskeletal orbitals (i.e., 10 × 6) of the 10 nickel atoms, from the total 150 electron count results in 30 skeletal CVEs. From a valence-bond viewpoint, these 15 skeletal electron pairs may be distributed as edge-localized bonds along the 15 Ni–Ni edges of the pentagonal nickel prism. This electron-precise configuration is analogous to that originally formulated[51] for the Ni_8 cube in **7**. The similarity between these three-connected nickel polyhedra is not surprising, especially if one considers that **6** may be formally derived from **7** via a one-Ni expansion of each of two opposite square faces in the Ni_8 core of **7** to two pentagonal faces in the Ni_{10} core of **6** together with the concurrent addition of one μ_4-PR ligand to the created square Ni_4 face, two terminal carbonyl ligands to the extra two nickel atoms, and two electrons to maintain electronic equivalence as a dianion. Each nickel atom in both **6** and **7** conforms to an 18-electron closed-shell electronic configuration.

King[52] recently proposed an equivalent treatment of the skeletal bonding in **7** in which the omnicapped cube was viewed as a 14-vertex $Ni_8(\mu_4\text{-P})_6$ deltahedron containing 24 triangular faces and 36 edges. Based upon the assumption that each tetracapped phosphorus atom is hypervalent and utilizes four internal valence orbitals (involving the additional use of the empty $3d_{x^2-y^2}$ AO) for bonding to the four nickel atoms and that each nickel utilizes six internal valence orbitals, the resulting 72 skeletal electrons (i.e., (6 × 4) + (8 × 6)) are the required number for edge-localized bonds along the 36 edges of the omnicapped cube.

Upon consideration of **6** as a 17-vertex $Ni_{10}(\mu_5\text{-P})_2(\mu_4\text{-P})_5$ deltahedron which has 30 triangular faces and 45 edges, a similar edge-localized bonding picture can be formulated. This model necessitates that each hypervalent μ_4-P atom utilizes four internal valence orbitals (involving the empty $3d_{x^2-y^2}$ AO), that each hypervalent μ_5-P utilizes five internal valence orbitals (involving the $3d_{x^2-y^2}$ and $3d_{xy}$ AOs), and that each nickel atom utilizes six internal valence orbitals in skeletal bonding. The resulting 90 skeletal electrons (i.e., (5 × 4) + (2 × 4) + (10 × 6) + 2) may be distributed among the 45 Ni–Ni and Ni–P edges as localized electron-pair bonds. Although the skeletal electron count appears to be consistent with edge-localized bonding, this proposed extreme type of skeletal cluster bonding is based upon the underlying assumption that the μ_4-P and μ_5-P atoms are hypervalent and contribute four and five internal valence orbitals, respectively, to the skeletal bonding. The use by each capping P atom of only its normal three internal valence orbitals gives rise to electron delocalization. Moreover, it is proposed herein that MO calculations performed with the nonparmetrized Fenske–Hall model[53] would yield electron-delocalized MOs which *cannot* be transformed into edge-localized Ni–Ni and Ni–P electron-pair bonds via application of the natural bond orbital procedure developed by Weinhold and co-workers[54] and altered by Kanis[55] to accommodate the results from the Fenske–Hall MO calculations. As an operational test of this hypothesis, Fenske–Hall MO calculations are planned.

Concluding Remarks. The stoichiometries of the reactants in these reactions were an essential factor for maximization of the product yields. If virtually any amount in excess of 1.5 equiv of $MePCl_2$ were used, a hexane soluble mixture would be obtained in addition to an increased amount of the toluene soluble portion, along with a decreased amount of the THF soluble mixture. An increased amount of $MePCl_2$ led to the formation of more highly oxidized species (i.e. less negative charge per cluster core atom)

(50) Gavney, J. A., Jr.; Underiner, T. L.; Dahl, L. F. To be submitted for publication.

(51) Lower, L. D.; Dahl, L. F. *J. Am. Chem. Soc.* **1976**, *98*, 5046–5047.

(52) King, R. B. *New J. Chem.* **1989**, *13*, 293–301.

(53) (a) Hall, M. B.; Fenske, R. F. *Inorg. Chem.* **1972**, *11*, 768–775. (b) Fenske, R. F. *Prog. Inorg. Chem.* **1976**, *21*, 179–208. (c) Fenske, R. F. *Pure Appl. Chem.* **1971**, *27*, 61–71.

(54) (a) Foster, J. P.; Weinhold, F. A. *J. Am. Chem. Soc.* **1980**, *102*, 7211–7218. (b) Rives, A. B.; Weinhold, F. A. *Int. J. Quantum Chem., Symp.* **1980**, *14*, 201–209; **1981**, *15*, 555. (c) Reed, A. E.; Weinstock, R. B.; Weinhold, F. A. *J. Chem. Phys.* **1985**, *83*, 735–746. (d) Reed, A. E.; Curtiss, L. A.; Weinhold, F. A. *Chem. Rev.* **1988**, *88*, 899–926.

(55) (a) Kanis, D. R. Ph.D. Thesis, University of Wisconsin—Madison, 1988. (b) Harris, H. A.; Kanis, D. R.; Dahl, L. F. *J. Am. Chem. Soc.* **1991**, *113*, 8602–8611.

and resulted in an increased phosphorus-to-nickel atom ratio in the cluster products. If less than 1 equiv of $MePCl_2$ were used, some unreacted **1** would be left. Of importance to this research was the separation of the THF extract of the reaction mixture by column chromatography which allowed characterization of the homologous $[Ni_{12-x}P_x(CO)_{24-3x}]^{2-}$ series (x = 2, 3, 4) and led to the isolation of the structurally related $[Ni_9P_3(CO)_{14}(PMe_2)]^-$ (**5**) and the structurally unprecedented heptacapped pentagonal prismatic Ni_{10} dianion, $[Ni_{10}(PMe)_7(CO)_{10}]^{2-}$ (**6**).

A comparative structural analysis of **2**, **3**, and **4** indicates that the observed geometric distortions are dictated by the smaller steric constraints of the PMe fragments relative to those of $Ni(CO)_3$ fragments. Spectroscopic and electrochemical characterization of the series revealed trends indicating a more electron-rich cluster core with increased PMe substitution. The observed trends upon going from **2** to **3** to **4** include the following: a lower terminal carbonyl IR frequency, a more negative oxidation potential, and higher field $^{31}P\{^1H\}$ NMR resonances. Solution $^{31}P\{^1H\}$ NMR spectra of **3** at 22 and 50 °C displayed a virtually identical ABX splitting with coupling constant values in agreement with its solid-state 1,2,12-Ni_9P_3 geometry; on this basis we rule out the possiblity of fluxional solution behavior occurring at room temperature in the icosahedral cores of these homologous anions. The ability of **2**, **3**, and **4** to adopt a noncentered icosahedral configuration is no doubt due to the electron-rich nature of the nickel atoms, as well as the formal replacement of two to four $Ni(CO)_3$ fragments by the smaller, isolobal methylphosphinidene groups. Thus, **2**, **3**, and **4** can each achieve an appropriate closed-shell 13 skeletal electron-pair count without overcrowding of the ligands and without requiring an interstitial atom.

Acknowledgment. We are most grateful to the National Science Foundation for its support of this research (Grant CHE-9013059). We are also indebted to Ms. Dana M. Benden (an Alfred L. Wilds Undergraduate Scholar in Chemistry, 1991–1992) for her help in preparing starting materials, to Dr. Gregory J. Lewis for his help in the chromatographic separation of the anionic nickel phosphinidine carbonyl clusters, and to Dr. Paul C. Vosejpka and Mr. Todd L. Underiner for their assistance in carrying out the NMR measurements.

Supplementary Material Available: Crystallographic tables for $[PPh_3Me]^+_2[Ni_{10}(PMe)_2(CO)_{18}]^{2-}$ (**2a**), $[PPh_3Me]^+_2[Ni_9(PMe)_3(CO)_{15}]^{2-}$ (**3a**), $[NMe_4]^+_2[Ni_9(PMe)_3(CO)_{15}]^{2-}\cdot{}^7/_6C_6H_{12}$ (**3b**), $[PPh_3Me]^+_2[Ni_8(PMe)_4(CO)_{12}]^{2-}\cdot C_6H_{12}$ (**4a**), $[Na(C_4H_8O)_4]^+[Ni_9(PMe)_3(CO)_{14}(\mu_2\text{-}PMe_2)]^-$ (**5a**), and $[PPh_3Me]^+_2[Ni_{10}(\mu_5\text{-}PMe)_2(\mu_4\text{-}PMe)_5(CO)_{10}]^{2-}\cdot C_4H_8O$ (**6a**) listing atomic coordinates and thermal parameters, selected interatomic distances, and bond angles (53 pages). Ordering information is given on any current masthead page.